frontiers in Earth Science

ORIGINAL RESEARCH
published: 09 March 2022
doi: 10.3389/feart.2022.864189

Quantitative Characterization for Pore Connectivity, Pore Wettability, and Shale Oil Mobility of Terrestrial Shale With Different Lithofacies—A Case Study of the Jurassic Lianggaoshan Formation in the Southeast Sichuan Basin of the Upper Yangtze Region in Southern China

Kun Zhang[1,2,3]*, Zhenxue Jiang[4,5], Yan Song[4,5,6], Chengzao Jia[6], Xuejiao Yuan[1,2], Xueying Wang[1,2], Liwen Zhang[1,2], Fengli Han[1,2], Yiming Yang[1,2], Yao Zeng[1,2], Pei Liu[1,2], Liangyi Tang[1,2], Xuecheng Chen[1,2] and Zehao Zheng[1,2]

[1]School of Geoscience and Technology, Southwest Petroleum University, Chengdu, China, [2]State Key Laboratory of Oil and Gas Reservoir Geology and Exploitation, Southwest Petroleum University, Chengdu, China, [3]Key Laboratory of Tectonics and Petroleum Resources, Ministry of Education, China University of Geosciences, Wuhan, China, [4]State Key Laboratory of Petroleum Resources and Prospecting, China University of Petroleum, Beijing, China, [5]Unconventional Petroleum Research Institute, China University of Petroleum, Beijing, China, [6]PetroChina Research Institute of Petroleum Exploration and Development, Beijing, China

OPEN ACCESS

Edited by:
Shu Jiang,
The University of Utah, United States

Reviewed by:
Tingwei Li,
Guangzhou Marine Geological Survey, China
Pengfei Wang,
China Geological Survey, China
Xin Li,
China National Offshore Oil Corporation, China

***Correspondence:**
Kun Zhang
shandongzhangkun@126.com

Specialty section:
This article was submitted to Economic Geology, a section of the journal Frontiers in Earth Science

Received: 28 January 2022
Accepted: 15 February 2022
Published: 09 March 2022

Citation:
Zhang K, Jiang Z, Song Y, Jia C, Yuan X, Wang X, Zhang L, Han F, Yang Y, Zeng Y, Liu P, Tang L, Chen X and Zheng Z (2022) Quantitative Characterization for Pore Connectivity, Pore Wettability, and Shale Oil Mobility of Terrestrial Shale With Different Lithofacies—A Case Study of the Jurassic Lianggaoshan Formation in the Southeast Sichuan Basin of the Upper Yangtze Region in Southern China. Front. Earth Sci. 10:864189. doi: 10.3389/feart.2022.864189

Some major hydrocarbon-bearing basins are rich in shale with terrestrial facies in China, which may provide abundant terrestrial shale oil and gas resources. This work studied the Jurassic Lianggaoshan Formation in the Southeast Sichuan Basin of the upper Yangtze Region. Core samples were chosen for the total organic carbon content and mineral composition analyses to classify shale lithofacies. Afterward, pore connectivity, pore wettability, and shale oil mobility with different lithofacies were characterized by spontaneous imbibition, nuclear resonance, and centrifugation. Conclusions are as follows: the pore connectivity of organic-rich clay shale was mostly between moderate to good with oil-prone wettability and high mobile oil saturation. The organic-rich mixed shale has moderate to good pore connectivity, water-prone wettability, and the highest mobile oil saturation. Organic matter–bearing clay shale has bad to moderate pore connectivity. Meanwhile, its pore wettability covers oil wetting, mixed wetting, oil-prone wetting, and water-prone wetting. Its mobile oil saturation was moderate. Regarding organic matter–bearing mixed shale, the pore connectivity was bad to moderate with mixed-wetting pore wettability and moderate mobile oil saturation.

Keywords: terrestrial shale, different lithofacies types, pore connectivity, pore wettability, shale oil mobility

1 INTRODUCTION

Huge achievements have been underscored in geological theories about unconventional oil and gas, horizontal drilling, fracturing technologies, and decreasing single-well drilling costs. In North America, the huge success in shale oil and gas exploration has reshaped the world energy landscape (Clarkson et al., 2013; Bazilian et al., 2014; Zhang et al., 2014; Geng et al., 2016; Hackley and Cardott, 2016). At the same time, China has achieved major progress in marine shale gas exploration in the Sichuan Basin and its surrounding areas, with shale gas fields built in Jiaoshiba, Weiyuan, Changning, Zhaotong, Luzhou, and other regions (Tan et al., 2014; Liu et al., 2018; Long et al., 2018; Xu et al., 2019; Yi et al., 2019). Some oil and gas-bearing basins in China, including Sichuan, Junggar, Bohai Bay, Songliao, and Ordos, are home to both marine and terrestrial strata, where terrestrial shale contains a large amount of potential shale oil and gas resources due to the moderate burial depth. At the same time, its thickness and total organic carbon (TOC) content are high with plentiful layers, moderate thermal evolution, and great Kerogen types. The convenience of exploration and high profits has attracted PetroChina and Sinopec to invest more in terrestrial light shale oil and to launch large-scale exploration activities (Li et al., 2018; Yang et al., 2019; Zhou et al., 2019; Zou et al., 2020; Li and Chen, 2021).

Shale pores serve as the primary reservoir space and seepage channel of light shale gas, and their connectivity as well as wettability are important research objects in studying a shale reservoir's characteristics because they affect the difficulty of oil and gas transportation in shale. Additionally, mobility is crucial to the evaluation of shale oil. The quantitative characterizations of connectivity, wettability, and shale oil mobility are essential. According to Huang et al. (2017), shale reservoirs have poorer pore connectivity than conventional oil and gas reservoirs; spontaneous imbibition is closely related to shale mineral composition; and foliation direction can affect spontaneous imbibition. Normally, the curve of spontaneous imbibition along the layers has a higher slope, but samples show that the curve through the layers has the same slope, which is probably because the higher hydrophilic mineral content in shale reservoirs weakens the directional dependence of water transportation in shale reservoirs. By analyzing the difference in pore space through nuclear magnetic resonance and high-pressure mercury intrusion porosimetry, Ning et al. (2017b) proposed a method for evaluating the pore connectivity of tight reservoirs based on experimental data and verified its correctness by spontaneous imbibition experiments. Jiang et al. (2020) studied terrestrial shale experimental tools including scanning electron microscope, Soxhlet extraction, gas adsorption, nuclear magnetic resonance, and centrifugation. They pointed out that pore structure characteristics and mineral composition of shale reservoirs jointly control the mobility of shale oil. Mobile oil is mainly reserved in large pores (>50 nm) and bound oil in small pores (<50 nm). Large pores offer space for shale oil reservoirs and contribute to shale oil flow, while small pores go against the move of shale oil owing to their larger pore-specific surface area, stronger adsorption capacity, and worse connectivity. The mineral composition has a significant impact on shale oil mobility. In addition, the bedding structure, such as the bedding fracture, is conducive to the development of reservoir space, which improves the shale pore connectivity and further promotes shale oil mobility.

This study explored pore structure characteristics of terrestrial shale with different lithofacies types, with the key exploration well TY1 being taken as the research object in the case analysis of terrestrial shale from the Jurassic Lianggaoshan Formation in the southeast Sichuan Basin of the upper Yangtze Region in southern China (**Figure 1**). This article is the first to classify lithofacies of shale in accordance with the TOC content and mineral composition. Afterward, experiments were conducted on shale samples: spontaneous imbibition was adopted to clarify the pore connectivity and wettability of shale with different lithofacies types; nuclear resonance and centrifugation were used to study the mobility of shale oil with different lithofacies types.

2 GEOLOGICAL SETTINGS

2.1 Sedimentary and Stratum Characteristics

The study area Lianggaoshan Fm. was divided into Liang Members I, II, and III, among which Liang Members I and II could be further divided into two sub-members, the upper and the lower (**Figure 2**). A set of gray siltstone, silty shale, black gray-gray black shale, and fine gray siltstone were found in the Lianggaoshan Formation. From the upper Liang Member I to the lower Liang Member II (Li et al., 2010; Li et al., 2017; Wang et al., 2018; Qing et al., 2019; Li X. et al., 2021), these sections were mainly deposited by gray-black shale deposits due to their favorable conditions for developing organic-rich shales. During the sedimentary period, the Lianggaoshan Formation went through a complete lake transgression and regression cycle. In the early period of Liang Member I, the resources were relatively sufficient before the lake transgression. Maximal flooding took place in the early period of Liang Member II, where the lake deposits were shallow to moderate. Afterward, the lake regression brought a favorable zone for the growth of organic-rich shale. In Liang Member III, coarse-grained clastic materials from the Delta Front were mainly deposited. Dark mud shales mainly existed in the upper Liang Member I and lower Liang Member II sections (Pang et al., 2019; Liu et al., 2020; Li C. et al., 2021).

2.2 Tectonic Characteristics

Located within the fold belt of the high-steep fault in eastern Sichuan, the study area is bordered by the faults of Huaying Mountain in the west, which is adjacent to the uplifts of central Sichuan, and by the fracture zone of Qiyue Mountain in the east, which sits between the Sichuan and Hubei provinces. With a series of arc-shaped mountains, the structural belt of the study area has a trending of regional structural lineament turning from NNE into NEE northward. The mountains within the structural belt form a high-steep anticline with the Permian–Triassic system at its core. The slow and steep sides are not asymmetrical. In general, the former has a stratum dip of 20°~30°, while that of the latter is 40°~70° or with an upside-down stratum. The wide valleys

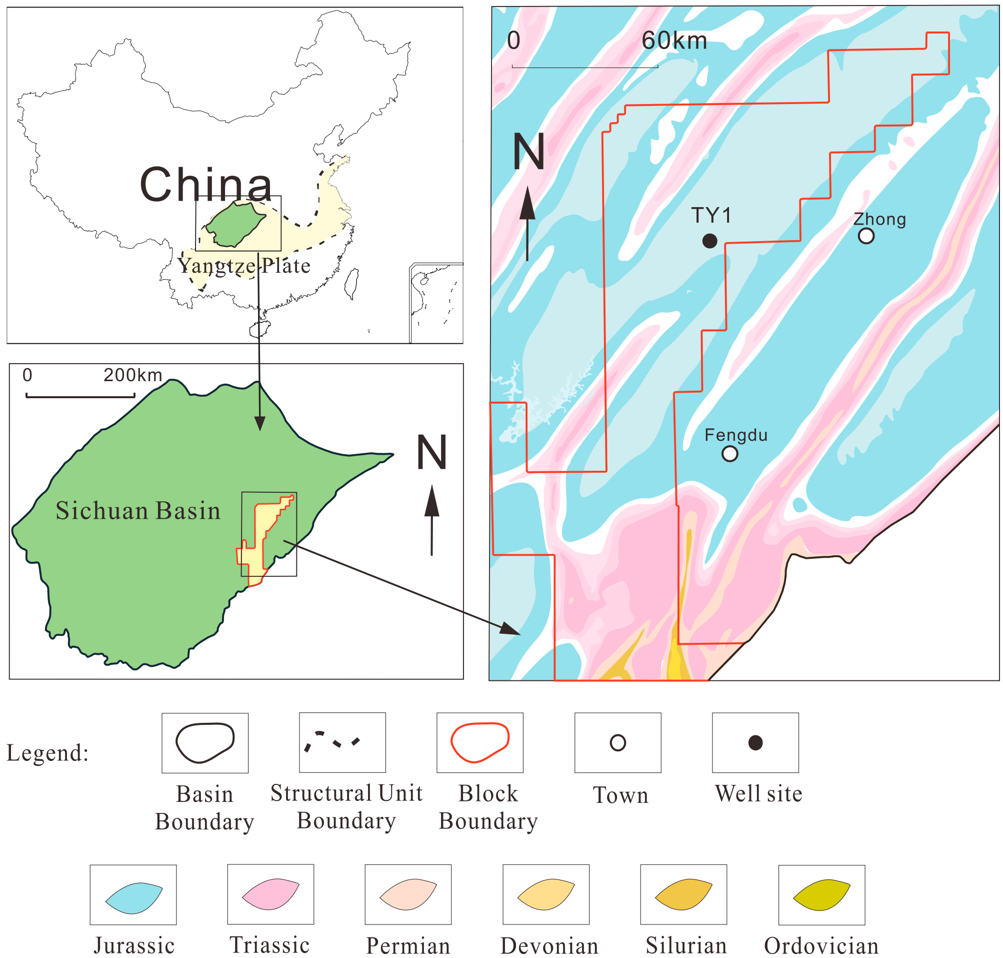

FIGURE 1 | Block location of the southeastern Sichuan Basin in southern China and distribution of the well TY1. Modified from references (Guo et al., 2016; Guo et al., 2017; Liu W. et al., 2021; Wei et al., 2021).

between the mountains are a wide and slow syncline composed of the Jurassic system as a typical barrier in structure and topography (Liu et al., 2010; Gao et al., 2017).

3 SAMPLES, EXPERIMENTS, AND DATA SOURCE

3.1 Total Organic Carbon Content and Mineral Component Analysis

A Sievers 860 TOC analyzer was used in the TOC content analysis for the same-depth samples, and a YST-I mineral analyzer was employed in the X-ray mineral-wide and clay mineral analysis. The results of the mentioned experiments were availed to classify the shale petrographic types.

3.2 Spontaneous Imbibition Experiment

Spontaneous imbibition refers to the process where a wetting fluid (water or oil) replaces a nonwetting fluid (air) under capillary force. Shale samples were selected in 15 depths of the TY1 well in the Lianggaoshan Formation. As shown in **Figure 3**, in each depth, two samples as a pair, respectively being horizontal and vertical to the bedding, were chosen to conduct the spontaneous imbibition experiment *via* water and oil (oil was replaced by decane). The numbering of experiment samples is as shown in **Table 1**, and experiment methods of spontaneous imbibition were as follows (Gao and Hu, 2015; Ning et al., 2017a; Wei et al., 2019; Zuo et al., 2019):

1) Shale samples of each depth were cut along the beddings into four 1 cm × 1 cm × 1 cm cubes, namely, A, B, C, and D. The top and the bottom of the cubes A and C were parallel, while those of B and D were vertical to the bedding. The other four sides of the samples were covered with epoxy resin (Zhang et al., 2019d; Wang G. et al., 2020; Gao et al., 2020).
2) The spontaneous imbibition experiment was conducted for 24 h. A and B used oil samples (decane), while water samples (deionized water) were adopted by C and D, as shown in the schematic diagram in **Figure 3**. The absorption content of oil and water was monitored by using an electronic balance.

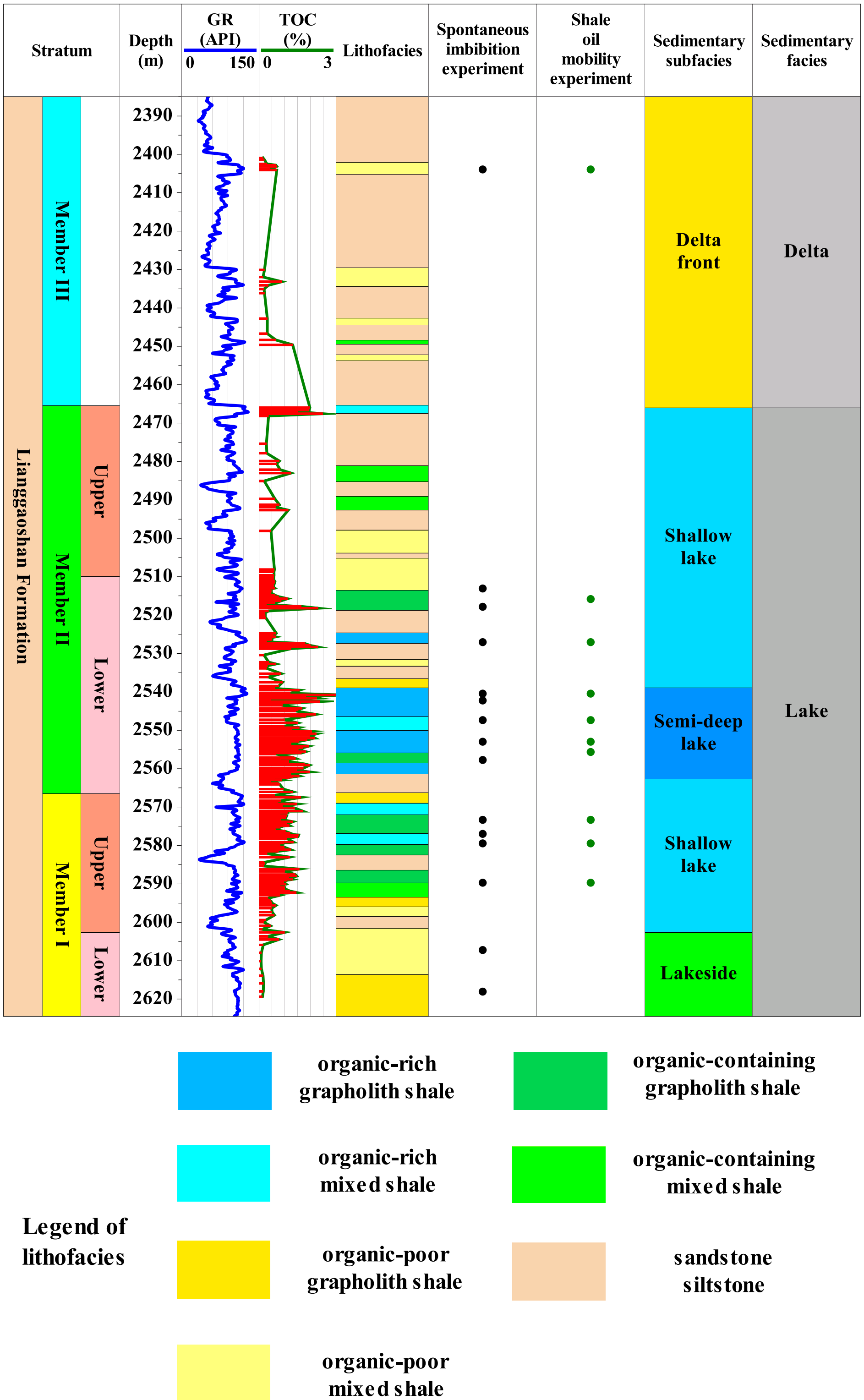

FIGURE 2 | The comprehensive stratigraphic column diagram of the Middle Jurassic Lianggaoshan Formation in the TY1 well. Modified from references (Liu W. et al., 2021; Wei et al., 2021).

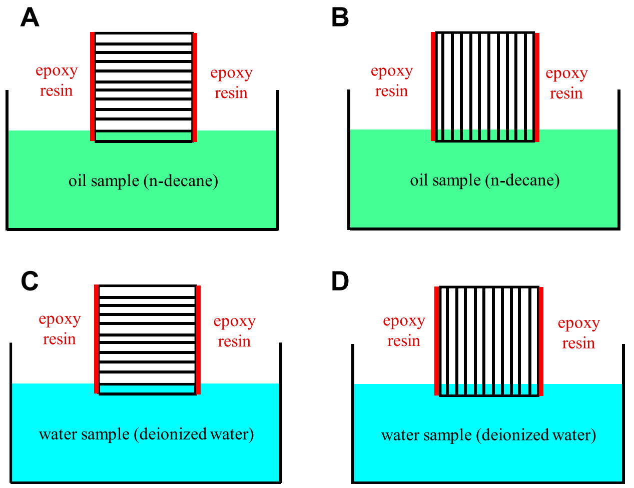

FIGURE 3 | Schematic diagram of samples with epoxy resin coating in the spontaneous imbibition experiment (black thin parallel lines refer to the shale foliation).

When the reading stabilized, the experiment ended. **Figure 4** shows the schematic diagram of the experiment devices (Liu and Zhang, 2019; Zhang et al., 2020a; Zhang et al., 2020b).

3) After the experiment, all data were presented into a spontaneous imbibition curve, where the axis x referred to time, and the axis y meant the water absorption height. Then, the slope of the spontaneous imbibition curve was calculated.

3.3 Experiment Analysis of Shale Oil Mobility

This study chose shale samples of 10 depths from the TY1 well in Lianggaoshan Fm. and conducted experiments on shale oil mobility with the combined methods of nuclear magnetic resonance (NMR) and centrifugation. The detailed steps are as follows, with the numbering of samples shown in **Table 2**.

Column samples were achieved by drilling holes with a diameter of 25 mm and a length below 60 mm. Samples were weighed before reaching the T_2 spectral line of original samples by NMR imaging (the first measurement of the T_2 spectral line) (Xie et al., 2019; Li et al., 2020; Zhang et al., 2022).

Vacuum pumping devices were used to obtain saturated water (-0.1Mpa). After about 6 h, the saturated samples were taken out and wiped with a moisturized tissue. Next, processed samples were weighed before measuring the T_2 spectral line in the NMR device (the second measurement of the T_2 spectral line; the general oil and water signal).

After processing the samples in the saturated manganese (Mn) for 72 h (to eliminate the water signal in the samples), we took them out and wiped the sample surface with wet tissues before weighing the saturated samples. Afterward, the T_2 spectral line of Mn-saturated samples was measured *via* NMR devices (the third measurement of the T_2 spectral line; oil signal). Oil saturation could be calculated based on the second and third measurement results.

Samples were put into the centrifuge. After an 8-hour 200psi centrifugation, the T_2 spectral line was measured again (the fourth measurement of the T_2 spectral line).

TABLE 1 | The depth and member of samples in the spontaneous imbibition experiment.

Number	Sample depth in the spontaneous imbibition experiment (m)	Formation
1	2,403.93	Liang Member III
2	2,513.07	Lower Liang Member II
3	2,517.83	Lower Liang Member II
4	2,527.04	Lower Liang Member II
5	2,540.45	Lower Liang Member II
6	2,542.24	Lower Liang Member II
7	2,547.35	Lower Liang Member II
8	2,552.98	Lower Liang Member II
9	2,557.73	Lower Liang Member II
10	2,573.32	Upper Liang Member I
11	2,576.98	Upper Liang Member I
12	2,579.45	Upper Liang Member I
13	2,589.7	Upper Liang Member I
14	2,607.23	Upper Liang Member I
15	2,618.06	Upper Liang Member I

Based on the centrifugation results, mobile oil saturation, bound oil saturation, and the T2 cutoff value were obtained.

A MesoMR12-025H core NMR analyzer was employed in the NMR logging. The multi-functional NMR analyzer has been widely used in geologic research and energy exploration. The magnets were permanent with a resonance frequency of 12.403 MHz. The temperature of the magnets was kept at 32.00 ± 0.02 °C, and the diameter of the sonde body was 25 mm.

4 RESULTS AND DISCUSSION

4.1 Lithofacies Types

Previous studies summarized several classification plans based on the TOC content and mineral constituents (Ji et al., 2016; Wang et al., 2016; Tang et al., 2017; Zhang et al., 2017; Zhang et al., 2019a). Based on the TOC content, shales can be divided into three groups, namely, organic-rich (TOC content ≥1.5%), organic-containing (TOC content ranges 1~1.5%), and organic-poor shale (TOC content ranges 0~1%) (Zhang et al., 2018b; Zhang et al., 2020c; Xiao et al., 2020; Guo et al., 2021; Shan et al., 2021). In terms of mineral contituents, shales can be classified into four types: calcareous (carbonate minerals ≥50%), grapholith (clay minerals ≥50%), siliceous (siliceous minerals ≥50%), and mixed shale (each mineral accounts for less than 50%) (Li et al., 2019; Huang H. et al., 2020; Xia et al., 2020; Chen et al., 2021). Combining the two classification standards, we can achieve three times four, that is, twelve lithofacies types based on the TOC content and mineral constituents, as shown in **Tables 3**, **4**.

4.2 Pore Connectivity and Wettability of Shale With Different Lithofacies Types

The curve slope of spontaneous imbibition can be used to evaluate the pore connectivity of shale reservoir properties (Zhang et al., 2018a; Huang J. et al., 2020; Liu et al., 2021a; Liu et al., 2021b). Previous studies have carried out simulations under the pore

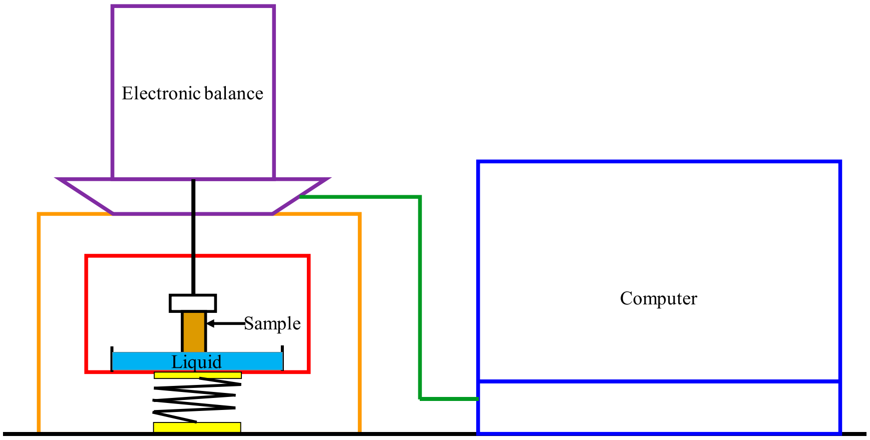

FIGURE 4 | Schematic Diagram of the spontaneous imbibition experiment devices.

TABLE 2 | The depth and members of samples in the shale oil mobility experiment.

Number	Depth of samples in the shale oil mobility experiment (m)	Formation
1	2,403.93	Liang Member III
2	2,515.82	Lower Liang Member II
3	2,527.04	Lower Liang Member II
4	2,540.45	Lower Liang Member II
5	2,547.35	Lower Liang Member II
6	2,552.98	Lower Liang Member II
7	2,555.65	Lower Liang Member II
8	2,573.32	Upper Liang Member I
9	2,579.45	Upper Liang Member I
10	2,589.7	Upper Liang Member I

TABLE 4 | Lithofacies types of shale samples in the shale oil mobility experiment.

Number	Depth of samples in the shale oil mobility experiment (m)	Lithofacies types
1	2,403.93	Organic-containing mixed shale
2	2,515.82	Organic-containing grapholith shale
3	2,527.04	Organic-rich grapholith shale
4	2,540.45	Organic-rich grapholith shale
5	2,547.35	Organic-rich mixed shale
6	2,552.98	Organic-rich grapholith shale
7	2,555.65	Organic-rich grapholith shale
8	2,573.32	Organic-rich mixed shale
9	2,579.45	Organic-containing grapholith shale
10	2,589.7	Organic-containing grapholith shale

TABLE 3 | Lithofacies types of shale in the spontaneous imbibition experiment.

Number	Sample depth in the spontaneous imbibition experiment (m)	Lithofacies types
1	2,403.93	Organic-containing mixed shale
2	2,513.07	Organic-poor mixed shale
3	2,517.83	Organic-containing grapholith shale
4	2,527.04	Organic-rich grapholith shale
5	2,540.45	Organic-rich grapholith shale
6	2,542.24	Organic-rich grapholith shale
7	2,547.35	Organic-rich mixed shale
8	2,552.98	Organic-rich grapholith shale
9	2,557.73	Organic-rich grapholith shale
10	2,573.32	Organic-rich mixed shale
11	2,576.98	Organic-containing grapholith shale
12	2,579.45	Organic-containing grapholith shale
13	2,589.7	Organic-containing grapholith shale
14	2,607.23	Organic-poor mixed shale
15	2,618.06	Organic-poor grapholith shale

network model and found that high pore connectivity (the average possibility of connectivity $p > 0.28$) corresponded to the spontaneous imbibition slope of 0.5. When $p = 0.2488$ (imbibition critical point), the spontaneous imbibition slope was 0.26. A lower slope means worse connectivity of porous media (Gao and Hu, 2013; Gao and Hu, 2016; Kang et al., 2019; Gao, 2021; Yu et al., 2022). **Table 5** shows the connectivity evaluation results. The spontaneous imbibition curve has two-stage features, where the slope in the early stage outnumbers that of the late period. Water absorption in the early stage resulted from the dry surface and rapid absorption of the bedding fracture, while that in the late stage was due to pore absorption characteristics. Imbibition curve slopes in the late stage were taken as the standard values.

Based on previous studies (Gao et al., 2018; Zhang N. et al., 2019; Wang, 2019; Wang J. et al., 2020; Hou et al., 2020), the rock wettability index was proposed and expressed in the following formula:

the rock wettability index: $W = (P_{water} - T_{water}) - (P_{oil} - T_{oil})$,where P_{water} refers to the spontaneous imbibition slope in

TABLE 5 | Evaluation of reservoir connectivity.

Slope	0~0.26	0.26~0.5	≥0.5
Connectivity evaluation	No imbibition Bad	Possible imbibition Moderate	Pores with high connectivity Good

TABLE 6 | Evaluation of rock wettability.

Wettability index W	≤–0.5	–0.5~0	0	0~0.5	≥0.5
Wettability evaluation	Water wetting	The closer to -0.5, the more water-prone wetting	Mixed wetting	The closer to 0.5, the more oil-prone wetting	Oil wetting

TABLE 7 | Connectivity and wettability evaluation of organic-rich grapholith shales and organic-rich mixed shales.

Depth		2,527	2,540.5	2,542	2,553	2,558	2,547	2,573
Lithofacies type		Organic-rich grapholith shales	Organic-rich grapholith shales	Organic-rich grapholith shales	Organic-rich grapholith shales	Organic-rich grapholith shales	Organic-rich mixed shales	Organic-rich mixed shalew
Member		Lower Liang II	Lower Liang II	Lower Liang II	Lower Liang II	Lower Liang II	Lower Liang II	Upper Liang I
Water	Parallel bedding	0.338	0.505	0.533	0.532	0.288	0.393	0.096
	Connectivity	Moderate	Good	Good	Good	Moderate	Moderate	Bad
	Vertical bedding	0.29	0.203	1.171	0.052	0.071	0.622	0.578
	Connectivity	Moderate	Bad	Good	Bad	Bad	Good	Good
Oil	Parallel bedding	0.242	0.343	0.424	0.394	0.42	0.416	0.442
	Connectivity	Bad	Moderate	Good	Moderate	Moderate	Moderate	Moderate
	Vertical bedding	0.408	0.327	0.415	0.233	0.103	0.169	0.204
	Connectivity	Moderate	Moderate	Moderate	Bad	Bad	Bad	Bad
Shale wettability index		0.214	0.286	–0.65	0.319	–0.1	–0.48	–0.72
Shale wettability evaluation		Oil-prone wetting	Oil-prone wetting	Water wetting	Oil-prone wetting	Mixed wetting	Water-prone wetting	Water wetting

a parallel direction with water as the fluid, T_{water} refers to the spontaneous imbibition slope in a vertical direction with water as the fluid, P_{oil} refers to the spontaneous imbibition slope in a parallel direction with oil as the fluid, and T_{oil} refers to the spontaneous imbibition slope in a vertical direction with oil as the fluid. **Table 6** shows the rock wettability based on the index (Zhang et al., 2019b; Zhang et al., 2019c).

The connectivity and the wettability index of samples 1–15 are presented in **Tables 7**, **8**. For organic-rich mixed, organic-rich grapholith, organic-containing grapholith, and mixed shale, the pore connectivity was mostly moderate to good. But most organic-poor shales had bad to moderate pore connectivity.

Organic-rich grapholith shales are mostly oil-prone wetting, and a few are water wetting and mixed wetting, while organic-rich mixed shales are water-prone wetting or water wetting. In terms of organic-containing grapholith shales, their wettability can be more complex, including oil, mixed, oil-prone, and water-prone wettability. The wettability of organic-containing mixed shales is mixed. Organic-poor grapholith shales are water wetting, while organic-poor mixed ones have water-prone or oil-prone wettability.

4.3 Evaluation of the Mobile Shale Oil With Different Lithofacies

4.3.1 Results of the Shale Oil Mobility Experiment

Tables 9, **10** show the findings from the shale oil mobility experiment. For the accumulative total oil porosity, the relaxation time of accumulative bound oil porosity is correlated with the T_2 cutoff value. Therefore, with the T_2 cutoff value, the cutoff diameter r can be calculated. Pores smaller than r represent bound oil reservoir spaces, while those larger represent mobile oil reservoir spaces. The cutoff diameter r can be calculated according to the following equation:

$R = \rho \times T_2 \times a$, where, based on the data provided by the laboratory, the value of a was set as 2 and shale surface relaxivity ρ as 10.

4.3.2 Evaluation of the Mobile Shale Oil

This chapter is a synthetical analysis of the experiment results. **Figure 5A** shows the average pore cutoff diameters of shales with different lithofacies types, which vary to quite a large extent. The pore cutoff diameters of organic-rich grapholith, organic-

TABLE 8 | Connectivity and wettability evaluation of organic-rich grapholith shales and organic-rich mixed shales.

Depth		2,517.8	2,577	2,579.5	2,589.7	2,403.9	2,618.1	2,513.1	2,607
Lithofacies type		Organic-containing grapholith shales	Organic-containing grapholith shales	Organic-containing grapholith shales	Organic-containing grapholith shales	Organic-containing mixed shales	Organic-poor grapholith shales	Organic-poor mixed shales	Organic-poor mixed shales
Member		Lower Liang II	Upper Liang I	Upper Liang I	Upper Liang I	Liang III	Lower Liang I	Lower Liang II	Lower Liang I
Water	Parallel bedding	0.344	0.551	0.371	0.256	0.356	0.218	0.372	0.2
	Connectivity	Moderate	Good	Moderate	Bad	Moderate	Bad	Moderate	Bad
	Vertical bedding	0.248	0.802	0.497	0.407	0.228	0.273	0.275	0.391
	Connectivity	Bad	Good	Moderate	Moderate	Bad	Moderate	Moderate	Moderate
Oil	Parallel bedding	0.179	0.106	0.074	0.257	0.449	0.889	0.263	0.083
	Connectivity	Bad	Bad	Bad	Bad	Moderate	Good	Moderate	Bad
	Vertical bedding	0.6283	0.265	0.535	0.275	0.391	0.19	0.199	0.593
	Connectivity	Good	Moderate	Good	Moderate	Moderate	Bad	Bad	Good
Shale wettability index		0.5453	−0.092	0.335	−0.133	0.07	−0.754	−0.102	0.32
Shale wettability evaluation		Oil wetting	Mixed wetting	Oil-prone wetting	Water-prone wetting	Mixed wetting	Water wetting	Water-prone wetting	Oil-prone wetting

TABLE 9 | Sample experiment results of theT2 cutoff value and pore cutoff diameter.

Number	Lithofacies type	T_2 cutoff calue (ms)	Pore cutoff diameter (nm)
1	Organic-containing mixed shales	0.42	8.4
2	Organic-containing grapholith shales	0.64	12.8
3	Organic-rich grapholith shales	0.6	12
4	Organic-rich grapholith shales	0.18	3.6
5	Organic-rich mixed shales	0.79	15.8
6	Organic-rich grapholith shales	0.3	6
7	Organic-rich grapholith shales	0.3	6
8	Organic-rich mixed shales	1.83	36.6
9	Organic-containing grapholith shales	0.24	4.8
10	Organic-containing grapholith shales	0.32	6.4

TABLE 10 | Experiment results of saturation of shale oil fluids.

Number	Depth (m)	Porosity (%)	Sample water saturation (%)	Sample oil saturation (%)	Fluid loss saturation (%)	Mobile oil saturation (%)	Bound oil saturation (%)
1	2,403.93	3.99	36.29	34.30	29.41	7.75	26.56
2	2,515.82	2.63	48.01	31.48	20.51	7.18	24.30
3	2,527.04	2.77	7.57	34.63	57.79	7.57	27.06
4	2,540.45	2.78	29.89	43.60	26.51	27.81	15.79
5	2,547.35	2.75	31.27	38.92	29.80	4.07	34.85
6	2,552.98	2.84	59.11	21.85	19.04	12.75	9.10
7	2,555.65	4.30	45.01	12.52	42.48	8.18	4.34
8	2,573.32	2.45	32.01	22.40	45.59	3.46	18.94
9	2,579.45	4.34	58.95	15.11	25.94	7.59	7.52
10	2,589.7	2.85	63.28	13.37	23.35	5.28	8.08

containing grapholith, and mixed shales were about 8 nm. Organic-rich mixed shales have a relatively large diameter of about 18 nm. Thus, it can be concluded that shale oil in 8–18 nm pores are mobile.

The pore fluid model used in this study is shown in **Figure 5B**. Water, fluid loss (natural gas, light hydrocarbon, and moisture dissipation), and oil (mobile and bound) exist in the shale pores. **Figure 5C** shows the average oil saturation of shales with different

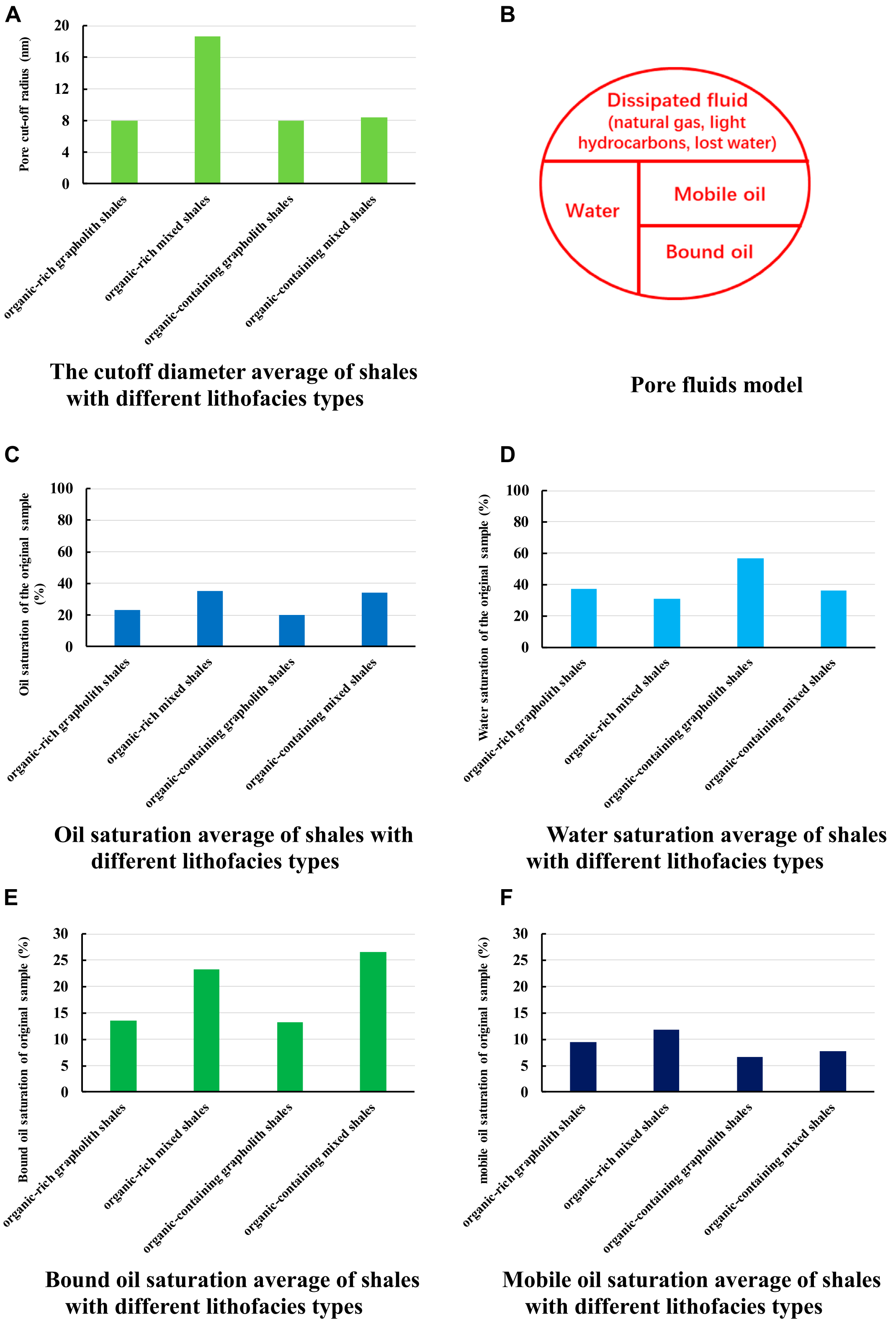

FIGURE 5 | Evaluation diagram of the shale pore cutoff diameter and pore fluids of shales with different lithofacies types. **(A)** The cutoff diameter average of shales with different lithofacies types. **(B)** Pore fluids model. **(C)** Oil saturation average of shales with different lithofacies types. **(D)** Water saturation average of shales with different lithofacies types. **(E)** Bound oil saturation average of shales with different lithofacies types. **(F)** Mobile oil saturation average of shales with different lithofacies types.

lithofacies types. Both organic-containing and organic-rich mixed shales have an oil saturation of about 35%, while the value for organic-rich and organic-containing grapholith shales is about 20%. According to **Figure 5D** presenting the average water saturation of different shales, organic-containing shales have the highest value, up to about 60%, while the water saturation of organic-rich grapholith, organic-rich mixed, and organic-containing mixed shales ranges from 30 to 40%.

Shale oil can be divided into mobile and bound types. According to **Figure 5E**, the bound oil saturation of organic-rich and organic-containing mixed shales is about 25%, while that of organic-rich and organic-containing grapholith shales is about 13%. The content of mobile oil determines the productivity of the shale oil well, as shown in **Figure 5F**. Organic-rich mixed shale has a mobile oil saturation of about 12%, and the mobile oil situation of organic-rich grapholith shale is 10%, which doubles that in organic-containing grapholith and organic-containing mixed shale with 6% of mobile oil saturation.

5 CONCLUSION

This study selected cores from the Jurassic Lianggaoshan Formation in the southeast Sichuan Basin of the upper Yangtze Region in southern China to analyze their TOC content and mineral constituents. Then, we divided shales into different lithofacies types and conducted the spontaneous imbibition, NMR, and centrifuge experiments to analyze pore connectivity, wettability, and shale mobility. The conclusions obtained are as follows:

1) The light shale oil in pores above 8–18 nm in size is mobile in shales of different lithofacies types.
2) The TOC content is the highest in organic-rich grapholith shales, mostly with moderate to good pore connectivity and comparably bad connectivity. Besides, the majority has oil-prone wettability, and the rest has water wettability. The mobile oil has high saturation. Overall, the TOC content is relatively high with moderate to good pore connectivity for organic-rich mixed shales, with a few shales having bad connectivity. The pores tend to be water-prone or water wetting with the highest mobile oil saturation.
3) The TOC content in organic-containing grapholith and mixed shales is moderate with bad-moderate pore connectivity mostly. A small number of the former type of shales have good connectivity. The wettability of organic-containing grapholith shales is complex, including oil, mixed, oil-prone, and water-prone wettability, while the organic-containing mixed shales are mixed wetting with moderate mobile oil saturation.
4) The TOC contents for organic-poor grapholith shales and mixed shales are low. Most shales have bad-moderate pore connectivity, with only a few possessing good connectivity. Besides, these shales are characterized by complex wettabilities, which include water wetting, oil-prone wetting, and water-prone wetting.

DATA AVAILABILITY STATEMENT

The raw data supporting the conclusion of this article will be made available by the authors, without undue reservation.

AUTHOR CONTRIBUTIONS

KZ, ZJ, YS, and CJ contributed to the conception and design of the study. KZ organized the database. ZJ performed the statistical analysis. KZ, ZJ, YS, and CJ wrote the first draft of the manuscript. XY, XW, LZ, FH, YY, YZ, PL, LT, XC, and ZZ wrote sections of the manuscript. All authors contributed to manuscript revision, read, and approved the submitted version.

FUNDING

This study was supported by the open funds from the National Natural Science Foundation of China (Nos 42102192, 42130803, and 42072174), the State Key Laboratory of Shale Oil and Gas Enrichment Mechanisms and Effective Development (G5800-20-ZS-KFGY012), the Shale Gas Evaluation and Exploitation Key Laboratory of Sichuan Province (YSK2022010), the open experiment fund of Southwest Petroleum University (2021KSP02029), the Open Fund of Key Laboratory of Tectonics and Petroleum Resources (China University of Geosciences), Ministry of Education, Wuhan (TPR-2020-07), the open funds from the State Key Laboratory of Petroleum Resources and Prospecting (PRP/open-2107), and the Science and Technology Cooperation Project of the CNPC-SWPU Innovation Alliance.

ACKNOWLEDGMENTS

We sincerely appreciate all reviewers and the handling editor for their critical comments and constructive suggestions.

REFERENCES

Bazilian, M., Brandt, A. R., Billman, L., Heath, G., Logan, J., Mann, M., et al. (2014). Ensuring Benefits from North American Shale Gas Development: Towards a Research Agenda. *J. Unconventional Oil Gas Resour.* 7 (7), 71–74. doi:10.1016/j.juogr.2014.01.003

Chen, D., Pang, X., Jiang, F., Liu, G., Pan, Z., and Liu, Y. (2021). Shale Oil Potential and Mobility of Low-Maturity Lacustrine Shales: Implications from NMR Analysis in the Bohai Bay Basin. *Energy Fuels* 35 (3), 2209–2223. doi:10.1021/acs.energyfuels.0c03978

Clarkson, C. R., Solano, N., Bustin, R. M., Bustin, A. M. M., Chalmers, G. R. L., He, L., et al. (2013). Pore Structure Characterization of North American Shale Gas Reservoirs Using USANS/SANS, Gas Adsorption, and Mercury Intrusion. *Fuel* 103 (103), 606–616. doi:10.1016/j.fuel.2012.06.119

Gao, F. (2021). Influence of Hydraulic Fracturing of strong Roof on Mining-Induced Stress Insight from Numerical Simulation. *J. Mining Strata Control. Eng.* 3 (2), 023032. doi:10.13532/j.jmsce.cn10-1638/td.20210329.001

Gao, J., Wang, X., He, S., Guo, X., Zhang, B., and Chen, X. (2017). Geochemical Characteristics and Source Correlation of Natural Gas in Jurassic Shales in the North Fuling Area, Eastern Sichuan Basin, China. *J. Pet. Sci. Eng.* 158, 284–292. doi:10.1016/j.petrol.2017.08.055

Gao, Z., and Hu, Q. (2013). Estimating Permeability Using Median Pore-Throat Radius Obtained from Mercury Intrusion Porosimetry. *J. Geophys. Eng.* 10 (2), 025014. doi:10.1088/1742-2132/10/2/025014

Gao, Z., Hu, Q., and Hamamoto, S. (2018). Using Multicycle Mercury Intrusion Porosimetry to Investigate Hysteresis Phenomenon of Different Porous Media. *J. Porous Media* 2018 (7), 21. doi:10.1615/jpormedia.2018017822

Gao, Z., and Hu, Q. (2015). Investigating the Effect of Median Pore-Throat Diameter on Spontaneous Imbibition. *J. Porous Media* 2015 (12), 18. doi:10.1615/jpormedia.v18.i12.60

Gao, Z., and Hu, Q. (2016). Wettability of Mississippian Barnett Shale Samples at Different Depths: Investigations from Directional Spontaneous Imbibition. *AAPG Bulletin*. 100 (1), 101–114. doi:10.1306/09141514095

Gao, Z., Fan, Y., Hu, Q., Jiang, Z., and Cheng, Y. (2020). The Effects of Pore Structure on Wettability and Methane Adsorption Capability of Longmaxi Formation Shale from the Southern Sichuan Basin in China. *Bulletin* 104 (6), 1375–1399. doi:10.1306/01222019079

Geng, J.-B., Ji, Q., and Fan, Y. (2016). The Impact of the North American Shale Gas Revolution on Regional Natural Gas Markets: Evidence from the Regime-Switching Model. *Energy Policy* 96, 167–178. doi:10.1016/j.enpol.2016.05.047

Guo, H., Ji, M., Sun, Z., and Zhou, Z. (2021). Energy Evolution Characteristics of Red sandstone under Cyclic Load. *J. Mining Strata Control. Eng.* 3 (4), 043019. doi:10.13532/j.jmsce.cn10-1638/td.20211008.001

Guo, X., Hu, D., Li, Y., Wei, Z., Wei, X., and Liu, Z. (2017). Geological Factors Controlling Shale Gas Enrichment and High Production in Fuling Shale Gas Field. *Pet. Exploration Dev.* 44 (4), 481–491. in Chinese with English abstract. doi:10.1016/s1876-3804(17)30060-5

Guo, X., Hu, D., Wei, Z., Wang, Q., and Zhang, H. (2016). Discovery and Exploration of Fuling Shale Gas Field. *China Pet. Exploration* 21 (3), 271–286. (in Chinese with English abstract). doi:10.4236/nr.2016.75024

Hackley, P. C., and Cardott, B. J. (2016). Application of Organic Petrography in North American Shale Petroleum Systems: A Review. *Int. J. Coal Geology.* 163, 8–51. doi:10.1016/j.coal.2016.06.010

Hou, E., Cong, T., Xie, X., and Wei, J. (2020). Ground Surface Fracture Development Characteristics of Shallow Double Coal Seam Staggered Mining Based on Particle Flow. *J. Mining Strata Control. Eng.* 2 (1), 013521. doi:10.13532/j.jmsce.cn10-1638/td.2020.01.002

Huang, H., Li, R., Jiang, Z., Li, J., and Chen, L. (2020a). Investigation of Variation in Shale Gas Adsorption Capacity with Burial Depth: Insights from the Adsorption Potential Theory. *J. Nat. Gas Sci. Eng.* 73, 103043. doi:10.1016/j.jngse.2019.103043

Huang, J., Jin, T., Chai, Z., Barrufet, M., and Killough, J. (2020b). Compositional Simulation of Three-phase Flow in Mixed-Wet Shale Oil Reservoir. *Fuel* 260, 116361. doi:10.1016/j.fuel.2019.116361

Huang, R., Jiang, Z., Gao, Z., Li, Y., Zhang, K., Zhang, X., et al. (2017). Effect of Composition and Structural Characteristics on Spontaneous Imbibition of Shale Reservoir. *Pet. Geology. Recovery Efficiency* 24 (1), 111–115. in Chinese with English abstract. doi:10.13673/j.cnki.cn37-1359/te.2017.01.017

Ji, W., Song, Y., Jiang, Z., Meng, M., Liu, Q., Chen, L., et al. (2016). Fractal Characteristics of Nano-Pores in the Lower Silurian Longmaxi Shales from the Upper Yangtze Platform, south China. *Mar. Pet. Geology.* 78, 88–98. doi:10.1016/j.marpetgeo.2016.08.023

Jiang, Z., Li, T., Gong, H., Jiang, T., Chang, J., Ning, C., et al. (2020). Characteristics of Low-Mature Shale Reservoirs in Zhanhua Sag and Their Influence on the Mobility of Shale Oil. *Acta Petrolei Sinica* 41 (12), 1587–1600. (in Chinese with English abstract). doi:10.7623/syxb202012011

Kang, H., Xu, G., Wang, B., Wu, Y., Jiang, P., and Pan, J. (2019). Forty Years Development and Prospects of Underground Coal Mining and Strata Control Technologies in China. *J. Mining Strata Control. Eng.* 1 (1), 013501. doi:10.13532/j.jmsce.cn10-1638/td.2019.02.002

Li, C., He, D., Lu, G., Wen, K., Simon, A., and Sun, Y. (2021a). Multiple Thrust Detachments and Their Implications for Hydrocarbon Accumulation in the Northeastern Sichuan Basin. *Southwestern China. AAPG Bull.* 105 (2), 357–390. doi:10.1306/07272019064

Li, D., Li, J., Zhang, B., Yang, J., and Wang, S. (2017). Formation Characteristics and Resource Potential of Jurassic Tight Oil in Sichuan Basin. *Pet. Res.* 2 (4), 301–314. doi:10.1016/j.ptlrs.2017.05.001

Li, J., Tao, S., Wang, Z., Zou,, C., Gao, X., and Wang, S. (2010). Characteristics of Jurassic Petroleum Geology and Main Factors of Hydrocarbon Accumulation in NE Sichuan basin. *Nat. Gas Geosci.* 2010, 5.

Li, J., Jiang, C., Wang, M., Lu, S., Chen, Z., Chen, G., et al. (2020). Adsorbed and Free Hydrocarbons in Unconventional Shale Reservoir: A New Insight from NMR T1-T2 Maps. *Mar. Pet. Geology.* 116 (116), 104311. doi:10.1016/j.marpetgeo.2020.104311

Li, J., Liu, Z., Li, J., Lu, S., Zhang, T., Zhang, X., et al. (2018). Fractal Characteristics of Continental Shale Pores and its Significance to the Occurrence of Shale Oil in China: a Case Study of Biyang Depression. *Fractals* 26 (02), 1840008. doi:10.1142/s0218348x1840008x

Li, M., and Chen, X. (2021). A Comparison of Geological Characteristics of the Main Continental Shale Oil in China and the US. *Lithosphere*. 2021 (Special 1), 3377705. doi:10.2113/2021/3377705

Li, M., Chen, Z., Ma, X., Cao, T., Qian, M., Jiang, Q., et al. (2019). Shale Oil Resource Potential and Oil Mobility Characteristics of the Eocene-Oligocene Shahejie Formation, Jiyang Super-depression, Bohai bay basin of China. *Int. J. Coal Geology.* 204 (204), 130–143. doi:10.1016/j.coal.2019.01.013

Li, X., Jiang, Z., Jiang, S., Wang, S., Miao, Y., Wu, F., et al. (2021b). Synergetic Effects of Matrix Components and Diagenetic Processes on Pore Properties in the Lower Cambrian Shale in Sichuan Basin, South China. *J. Nat. Gas Sci. Eng.* 94 (94), 104072. doi:10.1016/j.jngse.2021.104072

Liu, B., He, S., Meng, L., Fu, X., Gong, L., and Wang, H. (2021a). Sealing Mechanisms in Volcanic Faulted Reservoirs in Xujiaweizi Extension Northern Songliao Basin Northeastern China. *AAPG Bull.* 2021, 20210315. doi:10.1306/03122119048

Liu, B., Sun, J., Zhang, Y., He, J., Fu, X., Yang, L., et al. (2021b). Reservoir Space and Enrichment Model of Shale Oil in the First Member of Cretaceous Qingshankou Formation in the Changling Sag, Southern Songliao Basin, NE China. *Pet. Exploration Dev.* 48 (3), 608–624. doi:10.1016/s1876-3804(21)60049-6

Liu, W., Zhang, K., Li, Q., Yu, Z., Cheng, S., Liu, J., et al. (2021c). Quantitative Characterization for the Micronanopore Structures of Terrestrial Shales with Different Lithofacies Types: A Case Study of the Jurassic Lianggaoshan Formation in the Southeastern Sichuan Basin of the Yangtze Region. *Geofluids* 2021, 1416303. doi:10.1155/2021/1416303

Liu, X., and Zhang, D. (2019). A Review of Phase Behavior Simulation of Hydrocarbons in Confined Space: Implications for Shale Oil and Shale Gas. *J. Nat. Gas Sci. Eng.* 68, 102901. doi:10.1016/j.jngse.2019.102901

Liu, Y., Tang, X., Zhang, J., Mo, X., Huang, H., and Liu, Z. (2018). Geochemical Characteristics of the Extremely High thermal Maturity Transitional Shale Gas in the Southern North China Basin (SNCB) and its Differences with marine Shale Gas. *Int. J. Coal Geology.* 194, 33–44. doi:10.1016/j.coal.2018.05.005

Liu, Z., Chen, Y., Ni, C., Lu, W., and Xu, Z. (2010). *Characteristics of sandstone Reservoirs of Middle-Lower Jurassic in central Sichuan Area2010*. Science & Technology Edition: Journal of Southwest Petroleum University 32 (2), 35. doi:10.3863/j.issn.1674-5086.2010.02.007

Liu, Z., Liu, G., Hu, Z., Feng, D., Zhu, T., Bian, R., et al. (2020). Lithofacies Types and Assemblage Features of continental Shale Strata and Their Implications for Shale Gas Exploration: A Case Study of the Middle and Lower Jurassic Strata in the Sichuan Basin. *Nat. Gas Industry B* 7 (4), 358–369. doi:10.1016/j.ngib.2019.12.004

Long, S., Feng, D., Li, F., and Du, W. (2018). Prospect Analysis of the Deep marine Shale Gas Exploration and Development in the Sichuan Basin, China. *J. Nat. Gas Geosci.* 3 (4), 181–189. doi:10.1016/j.jnggs.2018.11.001

Ning, C., Jiang, Z., Gao, Z., Li, Z., Zhu, R., Su, S., et al. (2017b). Quantitative Evaluation of Pore Connectivity with Nuclear Magnetic Resonance and High

Pressure Mercury Injection: A Case Study of the Lower Section of Es_3 in Zhanhua Sag. *J. China Univ. Mining Tech.* 46 (3), 578–585. (in Chinese with English abstract). doi:10.13247/j.cnki.jcumt.000616

Ning, C., Jiang, Z., Gao, Z., Su, S., Li, T., Wang, G., et al. (2017a). Characteristics and Controlling Factors of Reservoir Space of Mudstone and Shale in Es3x in the Zhanhua Sag. *Mar. Pet. Geology.* 88, 214–224. doi:10.1016/j.marpetgeo.2017.08.025

Pang, Z., Tao, S., Zhang, Q., Zhang, T., Yang, J., Fan, J., et al. (2019). Enrichment Factors and Sweep Spot Evaluation of Jurassic Tight Oil in central Sichuan Basin, SW China. *Pet. Res.* 4 (4), 334–347. doi:10.1016/j.ptlrs.2019.05.001

Qing, Y. H., Lü, Z. X., Wu, J. Y., Yang, J. J., Zhang, S. L., Xiong, C. H., et al. (2019). Formation Mechanisms of Calcite Cements in Tight Sandstones of the Jurassic Lianggaoshan Formation, Northeastern Central Sichuan Basin. *Aust. J. Earth Sci.* 66 (5), 723–740. doi:10.1080/08120099.2018.1564935

Shan, S., Wu, Y., Fu, Y., and Zhou, P. (2021). Shear Mechanical Properties of Anchored Rock Mass under Impact Load. *J. Mining Strata Control. Eng.* 3 (4), 043034. doi:10.13532/j.jmsce.cn10-1638/td.20211014.001

Tan, J., Horsfield, B., Fink, R., Krooss, B., Schulz, H.-M., Rybacki, E., et al. (2014). Shale Gas Potential of the Major Marine Shale Formations in the Upper Yangtze Platform, South China, Part III: Mineralogical, Lithofacial, Petrophysical, and Rock Mechanical Properties. *Energy Fuels* 28 (4), 2322–2342. doi:10.1021/ef4022703

Tang, X., Jiang, Z., Jiang, S., Cheng, L., and Zhang, Y. (2017). Characteristics and Origin of *In-Situ* Gas Desorption of the Cambrian Shuijingtuo Formation Shale Gas Reservoir in the Sichuan Basin, China. *Fuel* 187 (187), 285–295. doi:10.1016/j.fuel.2016.09.072

Wang, G., Pang, Y., and Ren, H. (2020a). Intelligent Coal Mining Pattern and Technological Path. *J. Mining Strata Control. Eng.* 2 (1), 013501. doi:10.13532/j.jmsce.cn10-1638/td.2020.01.001

Wang, J. (2019). Sustainable Coal Mining Based on Mining Ground Control. *J. Mining Strata Control. Eng.* 1 (1), 013505. doi:10.13532/j.jmsce.cn10-1638/td.2019.02.003

Wang, J., Zhang, C., Zheng, D., Song, W., and Ji, X. (2020b). Stability Analysis of Roof in Goaf Considering Time Effect. *J. Mining Strata Control. Eng.* 2 (1), 013011. doi:10.13532/j.jmsce.cn10-1638/td.2020.01.005

Wang, P., Jiang, Z., Ji, W., Zhang, C., Yuan, Y., Chen, L., et al. (2016). Heterogeneity of Intergranular, Intraparticle and Organic Pores in Longmaxi Shale in Sichuan Basin, South China: Evidence from SEM Digital Images and Fractal and Multifractal Geometries. *Mar. Pet. Geology.* 72, 122–138. doi:10.1016/j.marpetgeo.2016.01.020

Wang, X., He, S., Guo, X., Zhang, B., and Chen, X. (2018). The Resource Evaluation of Jurassic Shale in North Fuling Area, Eastern Sichuan Basin, China. *Energy Fuels* 32 (2), 1213–1222. doi:10.1021/acs.energyfuels.7b03097

Wei, L., Gao, Z., Mastalerz, M., Schimmelmann, A., Gao, L., Wang, X., et al. (2019). Influence of Water Hydrogen on the Hydrogen Stable Isotope Ratio of Methane at Low versus High Temperatures of Methanogenesis. *Org. Geochem.* 128 (128), 137–147. doi:10.1016/j.orggeochem.2018.12.004

Wei, X., Zhang, K., Li, Q., Hu, D., Wei, Z., Liu, R., et al. (2021). Quantitative Characterization of Pore Space for the Occurrence of continental Shale Oil in Lithofacies of Different Types: Middle Jurassic Lianggaoshan Formation in southeastern Sichuan Basin of the Upper Yangtze Area. *Geofluids* 2021, 9906500. doi:10.1155/2021/9906500

Xia, Y., Lu, C., Yang, G., Su, S., Pang, L., and Ding, G. (2020). Experimental Study on Axial Fracture Cutting and Fracturing of Abrasive Jet in Hard Roof Hole. *J. Mining Strata Control. Eng.* 2 (3), 033522. doi:10.13532/j.jmsce.cn10-1638/td.20200522.001

Xiao, J., Hao, Q., Zhang, S., and Fan, S. (2020). Influence of Oil Well Casing on the Law of Strata Pressure in Working Face. *J. Mining Strata Control. Eng.* 2 (1), 013522. doi:10.13532/j.jmsce.cn10-1638/td.2020.01.003

Xie, X., Krooss, B. M., Littke, R., Amann-Hildenbrand, A., Li, M., Li, Z., et al. (2019). Accessibility and Mobility of Hydrocarbons in Lacustrine Shale: Solvent Flow-Through Extraction Experiments on Eocene Oil Shales from Bohai Bay Basin, Eastern China. *Org. Geochem.* 127, 23–36. doi:10.1016/j.orggeochem.2018.11.006

Xu, H., Zhou, W., Zhang, R., Liu, S., and Zhou, Q. (2019). Characterizations of Pore, mineral and Petrographic Properties of marine Shale Using Multiple Techniques and Their Implications on Gas Storage Capability for Sichuan Longmaxi Gas Shale Field in China. *Fuel* 241, 360–371. doi:10.1016/j.fuel.2018.12.035

Yang, Z., Zou, C., Hou, L., Wu, S., Lin, S., Luo, X., et al. (2019). Division of fine-grained Rocks and Selection of "sweet Sections" in the Oldest continental Shale in China: Taking the Coexisting Combination of Tight and Shale Oil in the Permian Junggar Basin. *Mar. Pet. Geology.* 109, 339–348. doi:10.1016/j.marpetgeo.2019.06.010

Yi, J., Bao, H., Zheng, A., Zhang, B., Shu, Z., Li, J., et al. (2019). Main Factors Controlling marine Shale Gas Enrichment and High-Yield wells in South China: a Case Study of the Fuling Shale Gas Field. *Mar. Pet. Geology.* 103, 114–125. doi:10.1016/j.marpetgeo.2019.01.024

Yu, X., Bian, J., and Liu, C. (2022). Determination of Energy Release Parameters of Hydraulic Fracturing Roof Near Goaf Based on Surrounding Rock Control of Dynamic Pressure Roadway. *J. Mining Strata Control. Eng.* 4 (1), 013016. doi:10.13532/j.jmsce.cn10-1638/td.20210908.001

Zhang, K., Jiang, S., Zhao, R., Wang, P., Jia, C., and Song, Y. (2022). Connectivity of Organic Matter Pores in the Lower Silurian Longmaxi Formation Shale, Sichuan Basin, Southern China: Analyses from Helium Ion Microscope and Focused Ion Beam Scanning Electron Microscope. *Geol. J.* 2022, 1–13. doi:10.1002/gj.4387

Zhang, K., Jiang, Z., Xie, X., Gao, Z., Liu, T., Yin, L., et al. (2018a). Lateral Percolation and its Effect on Shale Gas Accumulation on the Basis of Complex Tectonic Background. *Geofluids* 2018, 5195469. doi:10.1155/2018/5195469

Zhang, K., Li, Z., Jiang, S., Jiang, Z., Wen, M., Jia, C., et al. (2018b). Comparative Analysis of the Siliceous Source and Organic Matter Enrichment Mechanism of the Upper Ordovician–Lower Silurian Shale in the Upper-Lower Yangtze Area. *Minerals* 2018 (8), 283. doi:10.3390/min8070283

Zhang, K., Peng, J., Liu, W., Li, B., Xia, Q., Cheng, S., et al. (2020b). The Role of Deep Geofluids in the Enrichment of Sedimentary Organic Matter: a Case Study of the Late Ordovician-Early Silurian in the Upper Yangtze Region and Early Cambrian in the Lower Yangtze Region south China. *Geofluids* 2020, 8868638. doi:10.1155/2020/8868638

Zhang, K., Song, Y., Jiang, S., Jiang, Z., Jia, C., Huang, Y., et al. (2019b). Accumulation Mechanism of marine Shale Gas Reservoir in Anticlines: a Case Study of the Southern Sichuan Basin and Xiuwu Basin in the Yangtze Region. *Geofluids* 2019, 5274327. doi:10.1155/2019/5274327

Zhang, K., Jia, C., Song, Y., Jiang, S., Jiang, Z., Wen, M., et al. (2020a). Analysis of Lower Cambrian Shale Gas Composition, Source and Accumulation Pattern in Different Tectonic Backgrounds: A Case Study of Weiyuan Block in the Upper Yangtze Region and Xiuwu Basin in the Lower Yangtze Region. *Fuel* 263, 115978. doi:10.1016/j.fuel.2019.115978

Zhang, K., Jiang, Z., Yin, L., Gao, Z., Wang, P., Song, Y., et al. (2017). Controlling Functions of Hydrothermal Activity to Shale Gas Content-Taking Lower Cambrian in Xiuwu Basin as an Example. *Mar. Pet. Geology.* 85, 177–193. doi:10.1016/j.marpetgeo.2017.05.012

Zhang, K., Peng, J., Wang, X., Jiang, Z., Song, Y., Jiang, L., et al. (2020c). Effect of Organic Maturity on Shale Gas Genesis and Pores Development: A Case Study on marine Shale in the Upper Yangtze Region, South China. *Open Geosciences* 12, 1617–1629. doi:10.1515/geo-2020-0216

Zhang, K., Song, Y., Jia, C., Jiang, Z., Jiang, S., Huang, Y., et al. (2019a). Vertical Sealing Mechanism of Shale and its Roof and Floor and Effect on Shale Gas Accumulation, a Case Study of marine Shale in Sichuan basin, the Upper Yangtze Area. *J. Pet. Sci. Eng.* 175, 743–754. doi:10.1016/j.petrol.2019.01.009

Zhang, K., Song, Y., Jiang, S., Jiang, Z., Jia, C., Huang, Y., et al. (2019d). Shale Gas Accumulation Mechanism in a Syncline Setting Based on Multiple Geological Factors: An Example of Southern Sichuan and the Xiuwu Basin in the Yangtze Region. *Fuel* 241, 468–476. doi:10.1016/j.fuel.2018.12.060

Zhang, K., Song, Y., Jiang, S., Jiang, Z., Jia, C., Huang, Y., et al. (2019c). Mechanism Analysis of Organic Matter Enrichment in Different Sedimentary Backgrounds: A Case Study of the Lower Cambrian and the Upper Ordovician-Lower Silurian, in Yangtze Region. *Mar. Pet. Geology.* 99, 488–497. doi:10.1016/j.marpetgeo.2018.10.044

Zhang, L., Li, J., Li, Z., Zhang, J., Zhu, Z., and Bao, Y. (2014). Advancements in Shale Oil/Gas Research in North American and Considerations on Exploration for Lacustrine Shale Oil/Gas in China. *Adv. Earth Sci.* 29 (6), 700–711. doi:10.11867/j.issn.1001-8166.2014.06.0700

Zhang, N., Han, C., and Xie, Z. (2019e). Theory of Continuous Beam Control and High Efficiency Supporting Technology in Coal Roadway. *J. Mining Strata Control. Eng.* 1 (1), 013005. doi:10.13532/j.jmsce.cn10-1638/td.2019.02.004

Zhou, L., Pu, X., Han, W., zhao, X., Jin, F., Xiao, D., et al. (2019). Exploration Breakthroughs and Geological Characteristics of continental Shale Oil: A Case Study of the Kongdian Formation in the Cangdong Sag, China. *Mar. Pet. Geology.* 2019 (102), 544–556. doi:10.1016/j.marpetgeo.2018.12.020

Zou, C., Yang, Z., Sun, S., Zhao, Q., Bai, W., Liu, H., et al. (2020). "Exploring Petroleum inside Source Kitchen": Shale Oil and Gas in Sichuan Basin. *Sci. China Earth Sci.* 63 (7), 934–953. doi:10.1007/s11430-019-9591-5

Zuo, J., Yu, M., Hu, S., Song, H., Wei, X., and Shi, Y. (2019). Experimental Investigation on Fracture Mode of Different Thick Rock Strata. *J. Mining Strata Control. Eng.* 1 (1), 013007. doi:10.13532/j.jmsce.cn10-1638/td.2019.02.008

Conflict of Interest: The authors declare that the research was conducted in the absence of any commercial or financial relationships that could be construed as a potential conflict of interest.

Publisher's Note: All claims expressed in this article are solely those of the authors and do not necessarily represent those of their affiliated organizations, or those of the publisher, the editors, and the reviewers. Any product that may be evaluated in this article, or claim that may be made by its manufacturer, is not guaranteed or endorsed by the publisher.